


Impact of bicycle traffic on the Macroscopic Fundamental Diagram

Some empirical findings in Shanghai

Journal Article**Author(s):**

Huang, Yizhe; Sun, Daniel J.; Li, Aoyong; Axhausen, Kay W. 

Publication date:

2021

Permanent link:

<https://doi.org/10.3929/ethz-b-000444814>

Rights / license:

In Copyright - Non-Commercial Use Permitted

Originally published in:

Transportmetrica A: Transport Science 17(4), <https://doi.org/10.1080/23249935.2020.1832157>

Impact of bicycle traffic on the Macroscopic Fundamental Diagram: Some empirical findings in Shanghai

Yizhe Huang , DanielJian Sun , Aoyong Li & Kay W. Axhausen

To cite this article: Yizhe Huang , DanielJian Sun , Aoyong Li & Kay W. Axhausen (2020): Impact of bicycle traffic on the Macroscopic Fundamental Diagram: Some empirical findings in Shanghai, Transportmetrica A: Transport Science, DOI: [10.1080/23249935.2020.1832157](https://doi.org/10.1080/23249935.2020.1832157)

To link to this article: <https://doi.org/10.1080/23249935.2020.1832157>



Accepted author version posted online: 13 Oct 2020.



Submit your article to this journal [↗](#)



View related articles [↗](#)



View Crossmark data [↗](#)

Publisher: Taylor & Francis & Hong Kong Society for Transportation Studies Limited

Journal: *Transportmetrica A: Transport Science*

DOI: 10.1080/23249935.2020.1832157



Impact of bicycle traffic on the Macroscopic Fundamental Diagram: Some empirical findings in Shanghai

Yizhe Huang^{a,b}, Daniel(Jian) Sun^{a,c,*}, Aoyong Li^b, Kay W. Axhausen^b

^a *State Key Laboratory of Ocean Engineering, School of Naval Architecture Ocean and Civil Engineering, Shanghai Jiao Tong University, Shanghai 200240, China*

^b *Institute for Transport Planning and Systems, ETH Zurich, Zurich 8093, Switzerland*

^c *China Institute of Urban Governance, Shanghai Jiao Tong University, Shanghai 200240, China*

*Corresponding author at: A829, Ruth-Mulan Chu Chao Building, No. 800 Dongchuan Road, Shanghai, 200240 China Tel: (0086-21) 34206674

E-mail addresses: huangyz@sjtu.edu.cn (Y.Z. Huang), danielsun@sjtu.edu.cn (D.J. Sun), aoyong.li@ivt.baug.ethz.ch (A.Y. Li), axhausen@ivt.baug.ethz.ch (K.W. Axhausen)

Impact of bicycle traffic on the Macroscopic Fundamental Diagram: Some empirical findings in Shanghai

ABSTRACT

Interactions between bicycles and cars have attracted increasing attention during the recent years. This paper aims to investigate the impact of bicycle traffic on the macroscopic fundamental diagrams (MFDs) for urban car traffic. Based on the empirical data, we develop a Bicycle Congestion Index (BCI)-based functional form of MFD relating network bicycle flow and car flow reductions. A link-based method is also proposed to estimate the MFD, considering the

spilling behaviors of bicycles at the link level. The results indicate that the effect of bicycle traffic on car MFD varies with different traffic conditions and network features. Compared with car-only roads, it is more efficient to increase network car flow by installing physically separated facilities and reducing the number of spilling bicycles. To this end, various traffic management strategies may be applied in the city of Shanghai, such as lifting the ban of cyclists on the central city area, building physically connected facilities to existing segments, and enforcing stricter operational regulations and management on bicycle traffic.

Keywords: Macroscopic Fundamental Diagram (MFD); car-bicycle interaction; bicycle traffic; network level; spilling behavior

1 Introduction

Urban street networks are typically shared by different travel modes, including cars, buses, bicycles, and pedestrians, which interact with each other and compete for limited road space, as well as public financial subsidies (Sun and Elefteriadou, 2014; Nian et al., 2019). Usually, cyclists can ride on the exclusive bicycle facility if there is one. However, in many cases, bicycles would frequently conflict with car traffic and slow down car speeds. For example, a case study in Nanjing, China revealed that bicycles were prone to spill into car lanes for segments with on-street parking (Chen et al., 2017). Another case study in Nanjing and Ningbo, China found that bicycles would travel outside the bicycle lane to keep desired speeds if the bicycle volume was large (Gang et al., 2016). The interference of bicycles also cannot be avoided when cars and bicycles share the same road segments without separation facilities between the two traffic streams. For example, for car-bicycle shared roads in China (Chen and Wang, 2016) and cycling streets in The Netherlands (Wierbor et al., 2020), cars need to slow down or even match the speeds of bicycles when bicycles are present on these roads. Understanding these car-bicycle interactions is important for both safety and accessibility purpose.

The impact of bicycle traffic on car traffic has been explored from different perspectives, mainly including road safety (Duan et al., 2017; Lawrence et al., 2018; Schepers et al., 2011), travel behavior (Piatkowski et al., 2017; Silvano et al., 2016), and

traffic flow characteristics (Allen et al., 1998; Vasic and Ruskin, 2012; Chen et al., 2014; Luo et al., 2015; Chen and Wang, 2016; Gang et al., 2016; Chen et al., 2017; Chen et al., 2018; Wierbos et al. 2020). Plenty of studies have investigated the multimodal traffic flow characteristics at the intersection level or link level based on the cellular automata (CA) model. For example, Vasic and Ruskin (2012) proposed a car-bicycle model for both link level and intersections using the CA model. Luo et al. (2015) simulated the heterogeneous flow using the CA model and discussed the impact of spilling behavior of bicycle on car traffic at the link level. Gang et al. (2016) investigated the dispersion phenomenon of bicycle traffic at signalized intersections based on the CA model. Chen and Wang (2016) proposed the CA model to investigate the impact of bicycle traffic on car speeds along the roadside. Chen et al. (2017) simulated the lane-changing behavior of cyclists on segments with on-street parking and identified the conflicts between car and bicycles based on the CA model. Some recent studies used analytic methods to investigate traffic dynamics of car and bicycle traffic. For example, Yuan et al. (2019) and Wierbos et al. (2020) proposed the macroscopic flow models for mixed bicycle-car traffic and the models were validated by traffic simulations. Nevertheless, these existing methods have limitations in empirically evaluating the multimodal planning and schemes at the network level. More empirical data-driven methods are needed to quantify the car-bicycle interactions and evaluate the bicycle-related schemes. For instance, to mitigate bicycle-car conflicts, Shanghai has enforced a traffic separation scheme and started to restrict bicycles on certain major roads in the central city area (Xin, 1996), which raises some controversy. As bicycle traffic is prohibited in the car-only roads, cyclists need to dismount and walk with their bicycles or make a detour to avoid these roads. According to Zacharias (2002), both car and bicycle volume declined significantly after implementing the separation schemes. It is crucial to understand multi-modal interactions and quantify the impact of such separation schemes on the network traffic performance.

This study evaluates the impact of bicycle traffic on network car traffic performance based on a network-wide traffic modelling approach, named macroscopic fundamental diagram (MFD). MFD is a reproducible curve that relates traffic production and accumulation within a network, which was proposed by Daganzo (2007) and Geroliminis and Daganzo (2007). Compared with traditional forecasting methods, the basic idea of the MFD is to shift the modelling emphasis from microscopic predictions to macroscopic monitoring and control (Daganzo, 2007). Practically, the MFD can be estimated without full knowledges of the dynamic traffic assignment and accurate prediction of driver

behavior. By monitoring the state of MFD continuously, traffic managers can understand whether the network system is in a desired accessibility level (Geroliminis and Daganzo, 2008). The existence of MFD was first verified by computer simulation (Geroliminis and Daganzo, 2007) and then examined empirically by Geroliminis and Daganzo (2008). So far, empirical MFDs have been observed in many cities. For example, Chinese cities, including Shanghai (Huang et al., 2018a), Shenzhen (Ji et al., 2014), and Changsha (Beibei et al., 2016), and Zurich, Switzerland (Ambühl et al., 2017) have observed empirical MFDs in urban networks. Recently, Loder et al. (2019) investigated the relationship between network features and critical accumulations based on MFDs from more than 40 cities. To consider bi-modal interaction within car-bus networks, Zheng and Geroliminis (2013), Geroliminis et al. (2014), and Loder et al. (2017) extended the single-modal MFD to bi-modal MFD model, known as three-dimensional macroscopic fundamental diagram (3D-MFD). Using simulation methods, the 3D-MFD has been applied to road space distribution (Zheng and Geroliminis, 2013; Wei and Sun, 2018), parking pricing (Zheng and Geroliminis, 2016), and perimeter flow control (Ampuntolas et al., 2017; Ding et al., 2017). The empirical 3D-MFD model assists to understand multimodal interactions at an aggregated level, which has also been verified with empirical data in Zurich (Loder et al., 2017) and in a large-scale network in Shenzhen, China (Fu et al., 2018).

Although the idea of MFD is mode-abstract and could be applied to multi-modal urban networks (Daganzo, 2007), empirical MFDs so far have only considered pedestrians (Hoogendoorn et al., 2010; Taherifar et al., 2019) and motorized traffic, e.g., car and bus. The impact of bicycle traffic on MFD has received little attention in the literatures. The possible reasons include: (1) lacking of the fundamental basis of bicycle behavior; (2) lacking of the bicycle flow-related sensor data; (3) difficulty simulating cyclists' behavior; and (4) scarcity of the congested bicycle traffic data at the network level. With the emergence of innovative mobility services during the last few years, such as dockless bicycle-sharing, a tremendous amount of bicycle data are available, which may be combined with vehicle data to explore the interactions between bicycle and car traffic. This paper aims to explore the impact of bicycle traffic on car flow at the network level. More specifically, three tasks were included as follows: (1) quantifying car-bicycle interactions; (2) analyzing the relationship between bicycle-related facilities and car MFD; (3) quantifying the impact of bicycle flow on car MFD under various network features. Based on the results of MFD in this study, we can understand: (1) whether the

traffic performance of the study network is at a desired level; (2) the potential of improving the network flow by reducing car-bicycle interactions; (3) how to adjust the existing bicycle facilities and traffic schemes to effectively improve the network performance.

The remainder of the paper is structured as follows: Section 2 presents the research area and empirical data used in this study. In Section 3, a data-driven method and a link-based method are proposed to quantify the effect of bicycle traffic on car MFD. In Section 4, results from the data-driven method and the link-based method are provided and compared. Finally, conclusions and findings are discussed in Section 5.

2 Research Area and Data

2.1 Research area

The inner central area of Shanghai, with a scale around 80 km², was chosen as the subject area (see Figure 1), including 177 secondary roads and 110 arterial roads. Residential roads and urban expressways were not considered. Note that a certain number of roads within the area are operated as car-only facilities, with the layout shown as “Car-only Road” in Figure 1.

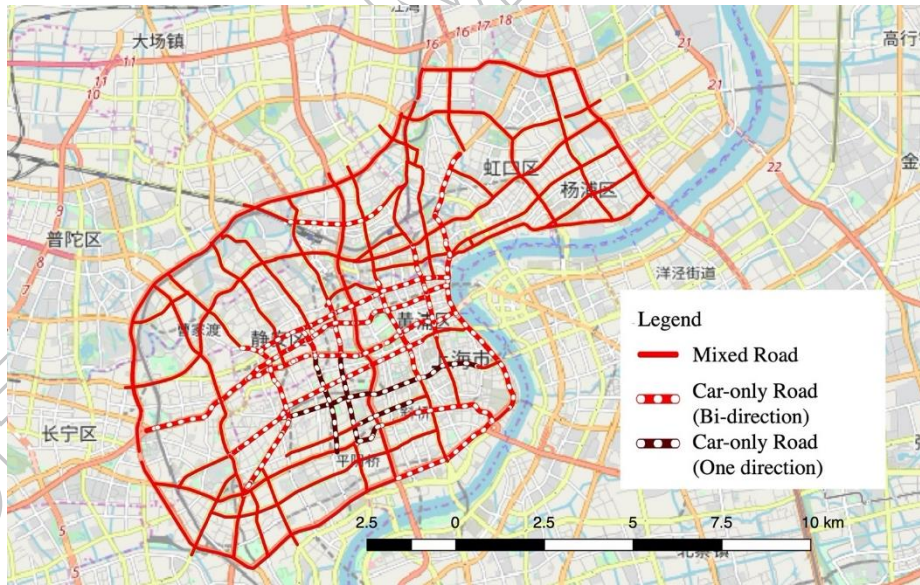


Figure 1. The study network in Shanghai (Source: OpenStreetMap)

2.2 Data

This section presents the empirical dataset used in the study, including taxi floating car data (FCD), loop detector data (LDD), GPS data from dockless sharing bicycles, and video data.

2.2.1 Car data

Sequential trajectories of floating car data (FCD) from Shanghai Qiang-Sheng Taxi Company were obtained from 13,475 taxis from Aug. 1 to 31, 2016. Each record contains taxi_ID, date, measurement_time, longitude, latitude, speed (km/h), and operational status (1 for vacant / 0 for occupied). The daily dataset has over one hundred million records in 10-second intervals (more than 10 GB). The data cleaning process is consistent with other studies (Huang et al., 2018b; Huang et al., 2018c; Sun and Ding, 2019). In Shanghai, the speed limits for most arterial roads and expressways are set from 60km/h to 100 km/h, as a result the records with the speed higher than 120 km/h were considered as outliers, and removed.

Loop detector data (LDD) was collected from 326 loop detectors by Shanghai traffic authorities, which are mainly installed on highways or ramps for traffic control purposes. The LDD dataset contains attributes including location (e.g., from one ramp to the other), road type (highway, on-ramp, or off-ramp), direction, hourly flow, and daily flow.

2.2.2 Bicycle Data

Bicycle data was obtained from Mobike Technology Company, one of the largest bicycle-sharing companies in China. As presented by Zhang and Mi (2018), Mobike receives about 20 million orders per day, accounting for nearly 60% market share of bicycle sharing. The dataset contains more than 1,000,000 bicycle-sharing orders in Shanghai from Aug. 1 to 31, 2016. Each record contains order_ID, bicycle_ID, user_ID, date, start_time, start_location, end_time, end_location, and trajectory points. Since each raw trajectory point k_s ($1 < s \leq n$) is not ordered and has no time stamps, the order of bicycle trajectories $\{\hat{k}_1, \hat{k}_2, \dots, \hat{k}_n\}$ was estimated by calculating and comparing relative distance between start_location \hat{k}_1 and end_location \hat{k}_n . For each trip u , the average speed \bar{v}_u was estimated by dividing the sum of adjacent distances $d_{s,s+1}$ by travel time T_u :

$$\bar{v}_u = \frac{\sum_{s=1}^{n-1} d_{s,s+1}}{T_u} \quad (1)$$

where $d_{s,s+1}$ is the Euclidean distance between two adjacent trajectory points \hat{k}_s and \hat{k}_{s+1} ; T_u is the travel duration between start_time and end_time for trip u . To estimate the travel distance and average speed for each trip u , the trajectory points out of the study network (e.g., residential roads) were also included.

The filtering criteria was carefully selected based on the quantile-based criteria (Park et al., 2003). Records with average speeds less than 5 km/h and higher than 25 km/h (close to the 5th percentile and 95th percentile of the overall travel speeds), or those with travel distance less than 500 meters, or more than 10 km (close to the 5th percentile and 95th percentile of the overall travel distance), were removed from the dataset.

2.2.3 Video Data

To validate the results from massive trajectories for car and bicycle traffic, we collected the traffic video data from ten selected segments (five physically separated segments and five non-physically separated segments) in Shanghai as in the previous study (Sun and Elefteriadou, 2010). Road and traffic flow information, such as separation type, green time/cycle length, car flow, bicycle flow, and number of spilling bicycles can be extracted from the video data. For each segment, we collect 2-hour video for peak hours (17:00 - 19:00) and 2-hour video for non-peak hours (13:00 - 15:00).

3 Methodology

This section focuses on the macroscopic traffic models for car-bicycle heterogeneous traffic. We first develop the data-driven method to empirically investigate the inference effect of bicycle traffic on car MFD. Then, the link-based method is built to explain and validate the effect of spilling bicycles on car traffic under various traffic conditions and road facilities.

3.1 Data-driven method

3.1.1 Stratified re-sampling method for MFD estimation

Previous studies have proved that spatial heterogeneity of traffic demand can cause flow reductions and make the shape of MFDs more scattered, such as Geroliminis and Sun (2011), Gayah and Daganzo (2011), Knoop et al. (2015), Xie et al. (2016), and Kim and Yeo (2017). Since this study mainly focuses on the effect of bicycle traffic and bicycle-related facilities on the shape of car MFDs, to reduce the influence of inhomogeneity of car demand, the stratified re-sampling method, is used for MFD estimation. As mentioned in Ambühl et al. (2018) and Loder et al. (2019), the upper-bound MFDs estimated from the re-sampling method describe the boundary of car traffic state and are relatively independent of car demand. The re-sampling method also effectively determines network

capacity and critical density, even if no distinct congested branch is observed (Ambühl et al., 2018).

In this study, to further investigate the impact of bicycle traffic on car MFD, we extend the re-sampling method to a stratified re-sampling method, which is illustrated in Figure 2. First, the study network is stratified into different sub-networks N_i . Each sub-network contains $|N_i|$ links with different facility types, such as number of lanes, road type, and separation type, which may assist to control the effect of these facility types when investigating the relationship between bicycle traffic and car MFD. Then, by following Ambühl et al. (2018), $|N_{i\Omega_j}|$ links are randomly drawn from each sub-network N_i without replacement and are combined into a sampled sub-network $N_{i\Omega_j}$ ($N_{i\Omega_j} \subset N_i$), where the ratio of $|N_{i\Omega_j}|/|N_i|$ denotes the given network share, such as 20%, 40%, 60%, and 80%. This process is repeated Ω_j times by re-selecting another $|N_{i\Omega_j}|$ links. For each subset of the original sub-network $N_{i\Omega_j}$, various empirical MFDs and corresponding network features may be obtained based on the empirical data. Finally, empirical MFDs from each sampled sub-network $N_{i\Omega_j}$ can be combined for different research purposes. For example, to compare the network performance among different sub-networks, empirical MFDs from sampled sub-networks $N_{i\Omega_j}$ can be combined into a re-sampled MFD for each sub-network N_i (see Section 4.1.1). To control the effect of network features and compare the effect of bicycle flow on car MFD for the total network N , these re-sampled MFDs can be further combined into a total re-sampled MFD (see Section 4.1.2). As mentioned in Ambühl et al. (2018), we can identify the stable upper-bound MFD from the re-sampled MFD or the total re-sampled MFD. Since road attributes for each sub-network are more homogeneous, the upper-bound MFDs in this study should have less heterogeneity-related flow reductions than the un-stratified network applied in Ambühl et al. (2018).

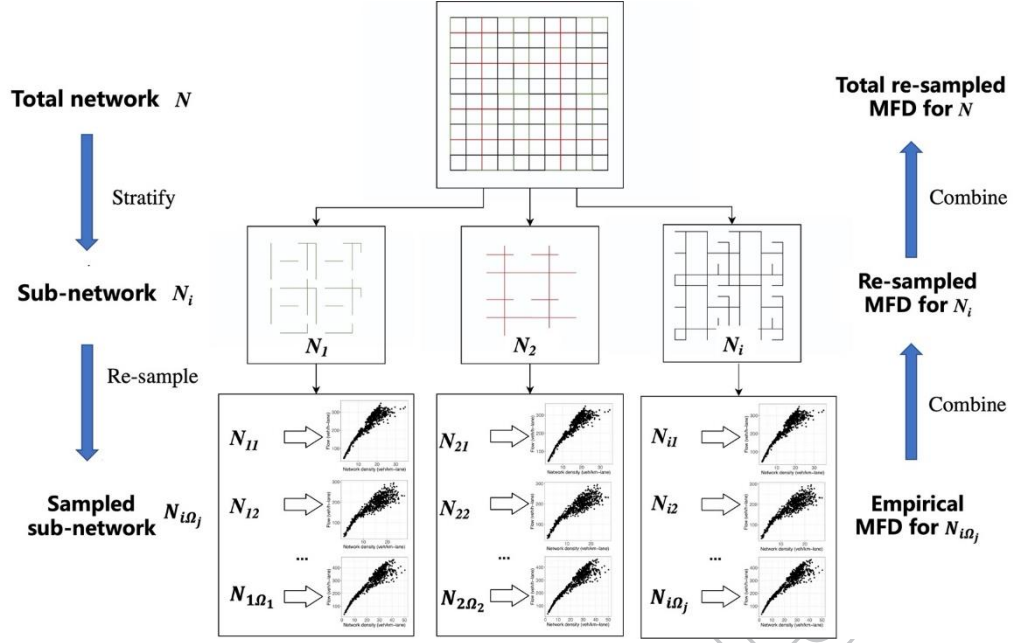


Figure 2. The stratified re-sampling method

Using the FCD of taxi trajectories, the empirical MFD for each sampled sub-network $N_{i\Omega_j}$ is estimated based on Edie's generalized traffic definition (Ambühl and Menendez, 2016; Edie, 1963). The total distance, d_{FCD}^{tot} , and the total travel time, t_{FCD}^{tot} , spend in the network during a 10-minute interval, are used to estimate the MFD:

$$\hat{q}_{FCD} = \frac{d_{FCD}^{tot}}{LT_{10}\hat{\rho}} \quad (2)$$

$$\hat{k}_{FCD} = \frac{t_{FCD}^{tot}}{LT_{10}\hat{\rho}} \quad (3)$$

where \hat{q}_{FCD} is the network flow estimated by FCD; \hat{k}_{FCD} is the network density estimated by FCD; L represents the length of total network, T_{10} represents a 10-minute time slice, and $\hat{\rho}$ represents taxi probe penetration rate.

Taxi probe penetration rate $\hat{\rho}$ is determined by combining the FCD and LDD for the same time slice. For each road segment i , loop detectors measure the link traffic flow q_i for each hour, which are then weighed by segment length l_i to calculate the network flow \hat{q}_{LDD} :

$$\hat{q}_{LDD} = \frac{\sum_i q_i l_i}{\sum_i l_i} \quad (4)$$

Since the network flow \hat{q}_{LDD} can also be expressed by the average of network flow \hat{q}_{FCD} estimated by FCD: $\hat{q}_{LDD} = \hat{q}_{FCD}$, the taxi penetration rate can then be estimated as:

$$\hat{\rho} = \frac{d_{FCD}^{tot}}{T_{10} \sum_i q_i l_i} \quad (5)$$

Note that the LDD used in this study are mainly installed on highways or ramps, the estimated taxi penetration rate, denoted as $\hat{\rho}_H$, is mainly suitable for the highway network instead of the surface road network. According to the 5th Shanghai Comprehensive Traffic Survey (2015), the average travel distance for each operational taxi trip is about 7.1 km, while for a regular car, it is about 14.5 km. Different travel distance may lead to other route preferences, which may result in varying taxi penetration rates between highways and surface roads. Therefore, the taxi penetration rate for surface roads, denoted as $\hat{\rho}_S$, should be further modified from the estimated taxi penetration rate for highways ($\hat{\rho}_H$). Details of modifying the taxi penetration rate can be found in Appendix 1.

3.1.2 BCI-based functional form for MFD

The first objective of this study is to identify whether the shape of car MFD will be affected by bicycle flow. Since the existing bicycle-sharing dataset has limitations in representing the total bicycle flow without information about the service penetration rate, the widely accepted V/C ratio (HCM2010, 2010) is not used to reflect the level of facilities service for the bicycle network. To this end, a Bicycle Congestion Index (BCI), defined as the relative volume of shared bicycles, is proposed to represent the relative bicycle flow characteristic for the target network. The value of BCI is calculated by normalizing the network volume of shared bicycles $Q_{shared-bicycle}$ into 0 to 1:

$$BCI = \frac{Q_{shared-bicycle}}{Q_{shared-bicycle}^{99th}} \quad (6)$$

To avoid outliers, the 99th percentile of the shared bicycle volume $Q_{shared-bicycle}^{99th}$ is used to present the maximum shared bicycle volume for the target network.

To quantify the impact of bicycle flow on car MFDs, a functional form may be proposed to capture the dynamics of car flow reduction due to bicycle traffic. Currently, most empirical MFD studies choose exponential-family or polynomial functions as the functional form of network flow-density relations. However, parameters of these methods do not have a strong physical meaning to explain the flow reduction of MFDs. Recently, Ambühl et al. (2020) proposed a new functional form of MFD to quantify the level of flow reduction, which was based on the smooth approximation of an upper bound of technologically feasible traffic states. The method measures the difference between observed traffic states and the trapezoidal MFD, which gives the values of potential to improve the existing network performance. This study uses the $\lambda - trapezoidal$ MFD

function to investigate the relationship between bicycle traffic and flow reductions of car MFD, as follows:

$$q_c(k_c, BCI) = -\lambda(BCI) \ln(\exp(-\frac{\mu_{f,c} k_c}{\lambda(BCI)}) + \exp(\frac{-Q_c}{\lambda(BCI)}) + \exp(\frac{-(\kappa_c - k_c)w_c}{\lambda(BCI)})) \quad (7)$$

where, q_c is the network car flow; k_c is the network car density; $\lambda(BCI)$ determines how far the observations of MFD lie beneath the trapezoidal MFD, which is assumed to be related to BCI in this study; $\mu_{f,c}$ is the free flow speed (car); Q_c is the intersection capacity (car); κ_c is the jam density (car); and w_c is the backward wave speed (car).

Technical parameters for trapezoidal MFD ($\mu_{f,c}$, Q_c , κ_c , and w_c) are estimated by empirical data or given by the local transportation authority. We estimate the free flow speed $u_{f,c}$ by using the 85th percentile of network taxi speeds for non-rush hours. The intersection capacity Q_c is calculated based on the equation given by Daganzo and Geroliminis (2008). The average ratio of green time/cycle length is given by Wang et al. (2014). The jam density κ_c is estimated by the average vehicle length. Here, we assume that the average vehicle length in Shanghai is similar to London and Marseille, where the value of κ_c is given by Ambühl et al. (2020). The backward wave speed w_c is provided by the local transportation authority. Technical parameters used in this paper are summarized as: $u_{f,c}=5.460$ m/s; $w_c=1.614$ m/s; $\kappa_c=0.150$ veh/m; $Q_c=0.175$ veh/s. To obtain MFDs with different values of the BCI , we estimate Eq. (7) using the non-linear quantile regression method, which allows to approximate the conditional quantiles of a response variable distribution. To avoid outliers' influence, we apply this method to estimate the upper-bound MFD (the 97.5th quantile). The *pseudo*- R^2 for the quantile regression estimation was calculated based on Koenker and Machado (1999).

3.2 Link-based method

To validate and explain the results of the data-driven method, this section proposed a link-based method that incorporating car-bicycle interactions at the disaggregated level.

3.2.1 Spilling behavior of bicycles

As bicycles are prone to spill into car lanes and hinder car traffic, the number of spilling bicycles is used to reflect car-bicycle conflicts for various traffic conditions and road facilities. In this study, bicycle facilities are classified into three categories according to the separation type between car and bicycle traffic (HCM2010, 2010):

- Bicycle lane: A portion of a roadway designated by striping, signing and pavement markings for preferential or exclusive use of bicycles.
- Bicycle path: A bicycle facility physically separated from motorized traffic by an open space or barrier, either within the highway right- of- way or within an independent right- of- way.
- Shared road: A facility where bicycles share a travel lane with motorized vehicular traffic.

Car-only roads are different from road segments with bicycle paths. Both car and bicycle traffic are allowed to use road segments with bicycle paths, while car-only roads are restricted for bicycle traffic, where cyclists should dismount and walk with the bicycles on sidewalks or make a detour.

In this study, spilling behavior of bicycles is modelled based on type of bicycle facilities and traffic conditions for both car and bicycle traffic. For segments with bicycle path or bicycle lane, according to the observations from video data, cyclists may spill into car lanes through the separation markings or gaps of disconnected separation facilities (e.g., the entrance of underground parking/companies/shopping malls) and hinder car traffic if the bicycle volume is large. Therefore, the number of spilling bicycles $q_{spill,i}$ is modelled based on the saturation level of bicycle facilities and the average car density during the 10-minute slice. For car-bicycle shared roads, the interference of bicycles cannot be avoided when cars passing bicycles. The number of spilling bicycles $q_{spill,i}$ is expressed as bicycle volume directly. For car-only roads, a small number of cyclists may spill into car lanes illegally if the local traffic laws and traffic management are not strict enough. The number of spilling bicycles for car-only roads is modelled based on network bicycle flow q_b and the percentage of cyclists violating the bicycle restricted rule δ . To sum up, the number of spilling bicycles per hour $q_{spill,i}$ is modelled for segments with different bicycle facilities $L_{b,i}$ as follows:

$$q_{spill,i} = \begin{cases} q_{b,i} * N_{b,i} * P_{spill,i}(k_{c,i}, q_{b,i}/C_{b,i}, s_i)|_{s_i=1} & \text{if } L_{b,i} \text{ is bicycle path} \\ q_{b,i} * N_{b,i} * P_{spill,i}(k_{c,i}, q_{b,i}/C_{b,i}, s_i)|_{s_i=0} & \text{if } L_{b,i} \text{ is bicycle lane} \\ q_{b,i} & \text{if } L_{b,i} \text{ is shared road} \\ q_b * \delta & \text{if } L_{b,i} \text{ is car_only road} \end{cases} \quad (8)$$

where $q_{spill,i}$ is the number of spilling bicycles per hour for segment i ; $q_{b,i}$ is the average bicycle volume for segment i (per lane); $N_{b,i}$ is the number of non-motorized lanes for

bicycle facility $L_{b,i}$; $P_{spill,i}$ is the percentage of spilling bicycles for bicycle facility $L_{b,i}$; $k_{c,i}$ is the average car density for segment i ; $C_{b,i}$ is the capacity of bicycle facility $L_{b,i}$; s_i is a dummy variable: $s_i=1$ for segments with bicycle path, $s_i=0$ for segments with bicycle lane; q_b is the average bicycle network volume; δ is the percentage of cyclists violating the bicycle restricted rule.

To simplify the model, the percentage of spilling bicycles $P_{spill,i}$ under the conditions of car density $k_{c,i}$, bicycle level of service ($q_{b,i}/C_{b,i}$), and separation type s_i is modelled using the linear regression model in this study:

$$P_{spill,i}(k_{c,i}, q_{b,i}/C_{b,i}, s_i) = \beta_0 + \beta_1 k_{c,i} + \beta_2 q_{b,i}/C_{b,i} + \beta_3 s_i \quad (9)$$

where β_0 , β_1 , β_2 and β_3 are coefficients to be estimated from the empirical data.

3.2.2 Spilling-based functional form for MFD

The interference effect of spilling bicycles on the fundamental diagram (FD) for car traffic is modelled based on the macroscopic flow model for mixed bicycle-car traffic (Wierbos et al., 2020). Similar to Luo et al. (2015), we assume that interactions between cars and bicycles are mainly for right-most car lanes. If the car lane $L_{c,i}$ is not the right-most lane, the Greenshields' linear model is adopted to model the car density $k_{c,i}$ and the car speed $v_{c,i}$. If the car lane $L_{c,i}$ is the right-most lane, similar to Wierbos et al. (2020), the interference effect of bicycle on $L_{c,i}$ can be divided into friction interference and block interference based on the average space $s_{spill,i}$ between two spilling bicycles. The average space $s_{spill,i}$ can be estimated by dividing the average speed of spilling bicycles $v_{spill,i}$ by the number of spilling bicycles per hour $q_{spill,i}$: $s_{spill,i} = 1/k_{spill,i} = v_{spill,i}/q_{spill,i}$. According to Wierbos et al. (2020), if the space between two spilling bicycles is sufficient on the right-most car lane ($s_{spill,i} > \alpha$), cars are more likely to overtake the spilling bicycles and the interference is mainly friction interference. If the space between two spilling bicycles is not large enough ($s_{spill,i} \leq \alpha$), the interference becomes mainly block interference and cars need to match bicycles' speed. The expressions of car speed $v_{c,i}^L$ on different lanes $L_{c,i}$ for segment i are given as follows:

$$v_{c,i}^L = \begin{cases} v_{f,i}(1 - k_{c,i}/k_{j,i}) & \text{if } L_{c,i} \text{ is not right - most lane} \\ v_{f,i}(1 - k_{c,i}/k_{j,i}) * \eta(s_{spill,i}) & \text{if } L_{c,i} \text{ is right - most lane, } s_{spill,i} > \alpha \\ \min(v_{spill,i}, v_{f,i}(1 - k_{c,i}/k_{j,i})) & \text{if } L_{c,i} \text{ is right - most lane, } s_{spill,i} \leq \alpha \end{cases} \quad (10)$$

where $v_{f,i}$ and $k_{j,i}$ are the free flow speed and the jam density for segment i ; the values of $v_{f,i}$ and $k_{j,i}$ are empirically estimated for segment i with a particular road type; $\eta(s_{spill,i})$ is the speed adjustment parameter for free flow speed of car due to the bicycle friction interference; α is the threshold between friction interference and block interference; $v_{spill,i}$ is the average speed of spilling bicycles.

Based on the speed-density relations for car traffic (Eq.10), the space-mean speed $v_{c,i}$ for segment i can be estimated as the average speed of each car lane. For given values of link density $k_{c,i}$ for each segments, the link traffic flow $q_{c,i}$ can be calculated as: $q_{c,i} = k_{c,i} * v_{c,i}$. Following Geroliminis and Daganzo (2008), for a given network, the network car flow q_c and network car density k_c can then be estimated by the length-weighted means of link flow and link density: $q_c = \sum_i q_{c,i} l_i / \sum_i l_i$; $k_c = \sum_i k_{c,i} l_i / \sum_i l_i$.

4 Results

In this section, we first compare the estimated MFDs for different road facilities using the data-driven method and the link-based method. Then, the effect of bicycle flow on car MFDs under different traffic conditions and road facilities are further investigated based on the two methods, respectively.

4.1 Data-driven method

Based on the stratified re-sampling method, we stratify the network into different sub-networks according to the segment features (e.g., road type, number of lanes, and separation type) and estimate the upper-bound MFD for each sub-network. The results of upper-bound MFD can be compared to investigate the effect of various road facilities and bicycle flow on car MFD. Then, we investigate the relationship between bicycle flow and car flow reductions based on the BCI-based functional form for car MFD.

4.1.1 Effect of road facilities

To compare re-sampled MFDs for different road types, the entire network is stratified into five sub-networks according to the road type and the number of car lanes of each segment: arterial roads with 2-4 lanes, with 5-6 lanes and with 7-10 lanes, secondary roads with 2-4 lanes and with 5-6 lanes. As mentioned in Ambühl et al. (2018), low network share (e.g., 20%) can increase the level of accuracy to estimate the critical points

of MFD. In this section, the network share $|N_{i\Omega_j}|/|N_i|$ is set to 20% and the number of draws Ω_j for each sub-network is set to 500 times. In other words, for each sampled sub-networks $N_{i\Omega_j}$, we randomly select 20% links without replacement from the sub-network N_i and estimate the network flow and density. This process is repeated 500 times by re-selecting another 20% links each time. Then, for each sub-network N_i , we identify stable upper-bound MFDs by combining empirical MFDs of each sampled sub-network $N_{i\Omega_j}$ and using the median of the top 50 flow values per density bin as the upper-bound flow. The capacity of each upper-bound MFD is determined by the 99th percentile of the network flow and the critical density is the average density corresponding to the capacity.

Similarly, to compare re-sampled MFDs for different separation types, the total network is stratified into six sub-networks according to the separation type and number of car lanes of each segment: car-only roads with 2-4 lanes and with 5-6 lanes; non-physically separated roads (segments with bicycle lane and shared lane) with 2-4 lanes and with 5-6 lanes; and physically separated roads (segments with bicycle path) with 2-4 lanes and with 5-6 lanes. Since the sample of shared lanes is not sufficient (10 segments within the network), we combine bicycle lanes and shared lanes (same bicycle capacity) and compare the results with other bicycle facilities. The network share $|N_{i\Omega_j}|/|N_i|$ is set to 20% and the number of draws Ω_j is set to 500 times for each sub-network.

The results of upper-bound MFD for different sub-networks are shown in Figure 3(a) and Figure 3(b). Since the congested branch for each upper-bound MFD is distinct, we can easily identify capacity and critical density for each sub-network (see Table 1). It is found that arterial roads with 7-10 lanes and secondary roads with 5-6 lanes have larger capacity reduction than other networks. Networks permitted for bicycle traffic have distinctly lower capacities compared to car-only networks. For the same density bin, networks with bicycle path have substantially higher car flow than networks without physically separated facilities.

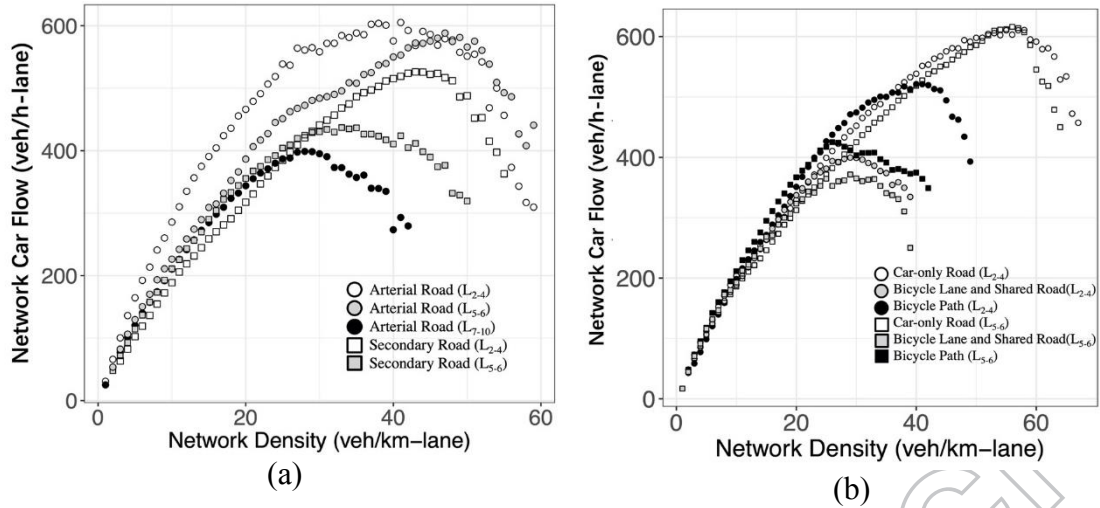


Figure 3. Relationship between facility type and upper-bound car MFDs: (a) road type with different number of lanes; (b) separation type with different number of lanes.

Table 1. Capacity (Q_{max}) and critical density (K_{cri}) for each sub-network

Road type/Separation type	# of car lanes	Q_{max} (veh/h-lane)	K_{cri} (veh/km-lane)
Arterial road	2 - 4	603.0	39.5
Arterial road	5 - 6	580.8	48.0
Arterial road	7 - 10	398.4	28.5
Secondary road	2 - 4	525.2	43.5
Secondary road	5 - 6	436.3	34.0
Car-only road	2 - 4	610.5	55.5
Car-only road	5 - 6	614.8	55.8
Non-physically separated road	2 - 4	399.4	29.5
Non-physically separated road	5 - 6	369.8	29.5
Physically separated roads	2 - 4	521.2	41.0
Physically separated roads	5 - 6	424.7	26.5

It should be noted that the effect of separation type was not controlled in Figure 3(a) and the effect of road type was not controlled in Figure 3(b). For example, sub-network with car-only roads consists of 25% arterials (speed limit: 50-60 km/h) and 75% secondary roads (speed limit: 30-40 km/h). The sub-network with bicycle path and non-physically separated roads includes 59.2% and 21.1% arterial roads, respectively. Different proportions of road type for each sub-network may lead to bias when comparing the shapes of MFD. The effect of road and separation types were controlled in Section 4.2.2 when applying the link-based method.

4.1.2 Relationship between bicycle flow and MFD

By using the stratified re-sampling method, we compare network density-flow relationship and network density-speed relationship while controlling for the bicycle flow

(BCI). To control the effect of car lanes, the general partition of network is based on the number of car lanes. The total network is divided into three sub-networks according to the number of car lanes. The first sub-network includes 143 segments ($|N_1| = 143$); the number of car lanes for each segment is two to four (two directions). The second sub-network has 101 segments ($|N_2| = 101$) with five to six lanes (two directions). The third sub-network has 43 segments ($|N_3| = 43$). Each segment has more than, or equal to, seven lanes (two directions). The network share $|N_{i\Omega_j}|/|N_i|$ is set to 20%. Different from Section 4.1.1, the number of draws Ω_j in this section is determined by the number of links for each sub-network: $\Omega_j = \lceil \frac{|N_i|}{|N|} \Omega \rceil$, where $|N_i|$ is the number of links for sub-network N_i ; $|N|$ is the number of links within the total network ($|N| = 287$); Ω is the total number of draws ($\Omega = 500$ times). Then, empirical car MFDs and bicycle volume are estimated for each sampled sub-network $N_{i\Omega_j}$. By combining results of each sampled sub-network, different combinations of bicycle flow (BCI), network features, and corresponding upper-bound MFDs (total re-sampled MFD) can be obtained.

We first compare the upper-bound MFDs for different groups of BCIs (see Figures 4(a) and 4(b)). It turns out that the bicycle flow has a negative impact on car MFDs. High BCI reduces network car capacity substantially and slows cars. Figures 4(c) and 4(d) compare the variance of network car flow and the variance of car speed with various network car density. High values of variance for network car flow are found in the high network car density branch and high values of variance for car speed are found in the low network car density branch. To compare the significance of upper-bound MFDs for different BCIs, sign tests and t-tests for paired sample (same network density) are carried out. The results of sign tests show that differences of MFD among each group of BCI are statistically significant at the 99% level of significance ($p < 0.01$). The results of paired t-test show that except for the insignificant difference of BCI (0.0-0.2) and BCI (0.2-0.4) ($p = 0.74$), the differences of MFD among other groups of BCI are significant at the 99% level ($p < 0.01$). Since more than 70% segments within the network are physically separated or car-only, the results are expected when the difference of MFDs for traffic conditions with the low bicycle volume and high car density are not significant.

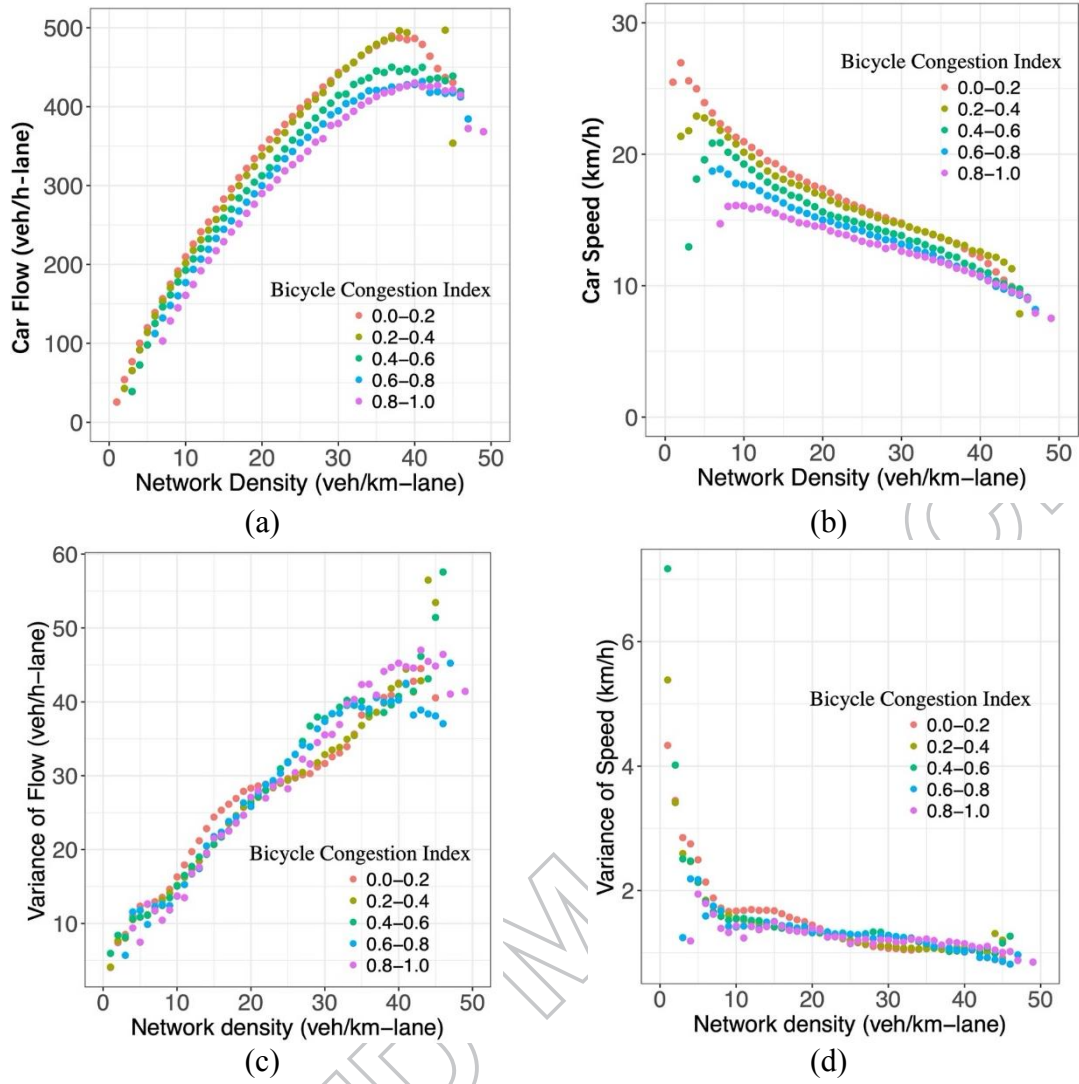


Figure 4. Car MFDs for various BCIs: (a) network density-flow relation; (b) network density-speed relation; (c) network density-variance of flow relation; (d) network density-variance of speed relation.

The results of Figure 4 are also confirmed by Figures 5(a) and 5(b), the contour plots of BCI and network car density. Figure 5(a) presents the critical density of cars for different values of BCI. The maximum network flow occurs when the network density is around 45 veh/km-lane and the BCI is approximately 0.3. As the empirical data are used, the correlation between bicycle demand and car demand may account for the reason that the maximum network flow value occurs when the bicycle flow is non-zero. The network car speed decreases as car density and BCI increases, which is in line with car-bicycle conflicts at the link level (Chen et al., 2018).

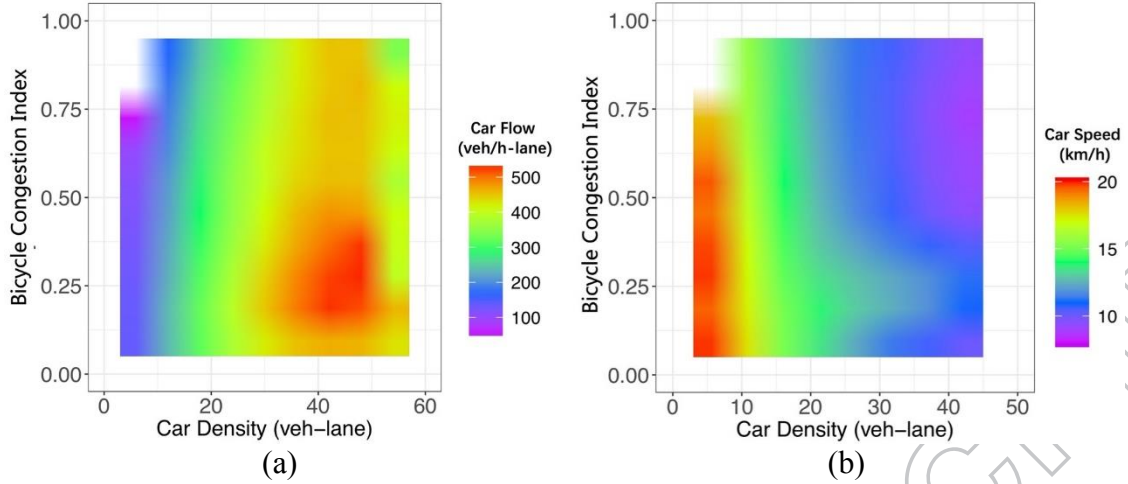


Figure 5. (a) Contour plot of network car flow; (b) Contour plot of network car speed

4.1.3 Relationship between bicycle flow and car flow reduction

Based on the BCI-based functional form for MFD (Eq. 7), the level of network car flow reduction (λ) can be estimated for different BCIs. In this section, the evolution of λ with respect to bicycle flow (BCI) under different network features is investigated, with the value of λ estimated in each BCI interval from corresponding car density and flow. The partition of network is consistent with Section 4.1.2 and the non-linear quantile regression method (the 97.5th quantile) is applied to estimate λ for the same shape parameters of trapezoidal MFD.

The estimation results of λ for different BCIs and the sensitivity of results to the network share are shown in Table 1. Values of λ for each group are between 0.03 to 0.07, which is reasonable according to Ambühl et al. (2020). Similar to the results in Figure 4, the value of λ is highly related to BCI, indicating that high bicycle flow may lead to large flow reductions in the MFD. *Pseudo-R*² values of 0.85-0.95 (close to 1) indicate a decent model fit for different BCIs and network shares. The corresponding estimated λ – *trapezoidal* MFDs for different values of BCI are shown in Figure A2, where the level of flow reduction for MFDs with different BCIs is observed.

Table 2. Estimation results of λ for different BCIs.

Network share	BCI	λ	t value	p	<i>pseudo-R</i> ²	N
20%	0.0 – 0.2	0.033	245.478	<0.001	0.901	505,932
	0.2 – 0.4	0.041	447.777	<0.001	0.895	376,038
	0.4 – 0.6	0.048	509.341	<0.001	0.858	155,352
	0.6 – 0.8	0.054	431.923	<0.001	0.862	59,994
	0.8 – 1.0	0.056	238.702	<0.001	0.862	24,576

40%	0.0 – 0.2	0.035	312.826	<0.001	0.907	456,960
	0.2 – 0.4	0.044	726.049	<0.001	0.905	392,700
	0.4 – 0.6	0.049	653.767	<0.001	0.861	173,424
	0.6 – 0.8	0.058	642.822	<0.001	0.863	69,288
	0.8 – 1.0	0.062	546.240	<0.001	0.860	30,288
60%	0.0 – 0.2	0.035	259.024	<0.001	0.909	446,016
	0.2 – 0.4	0.044	696.753	<0.001	0.906	390,540
	0.4 – 0.6	0.049	789.326	<0.001	0.862	181,656
	0.6 – 0.8	0.060	779.456	<0.001	0.864	72,444
	0.8 – 1.0	0.065	796.774	<0.001	0.859	32,004
80%	0.0 – 0.2	0.036	299.599	<0.001	0.908	476,022
	0.2 – 0.4	0.045	851.112	<0.001	0.907	367,686
	0.4 – 0.6	0.050	831.540	<0.001	0.861	179,346
	0.6 – 0.8	0.061	1,106.305	<0.001	0.869	69,282
	0.8 – 1.0	0.067	844.047	<0.001	0.852	30,324

Since the variations of λ for different BCIs can be used as a measure of car flow reduction, to further investigate the relationship between network bicycle flow (BCI) and car flow reduction, the values of λ are estimated in each BCI interval (0.01) from corresponding car density and flow. The relationship between BCI and λ for different network shares (20%, 40%, 60%, 80%) are shown in Figure 6(a). Similar to the results in Table 2, the values of λ with low network shares is slightly smaller than the values with high network shares for the same level of BCI, because road combinations with homogeneous traffic and less capacity reduction can be identified easily for smaller sampled sub-networks. The results also confirm that the growth of BCI can significantly increase the value of λ , indicating that the car infrastructure is increasingly inefficiently used due to bicycle traffic interference. When BCI is large enough (around 0.75), the values of λ become relatively stable, which is in line with Chen et al. (2018), who conclude that bicycle density impact on car delays becomes stable when bicycle density reaches a certain level. The trend of λ is similar for different network shares; the following analysis uses the 20% network share.

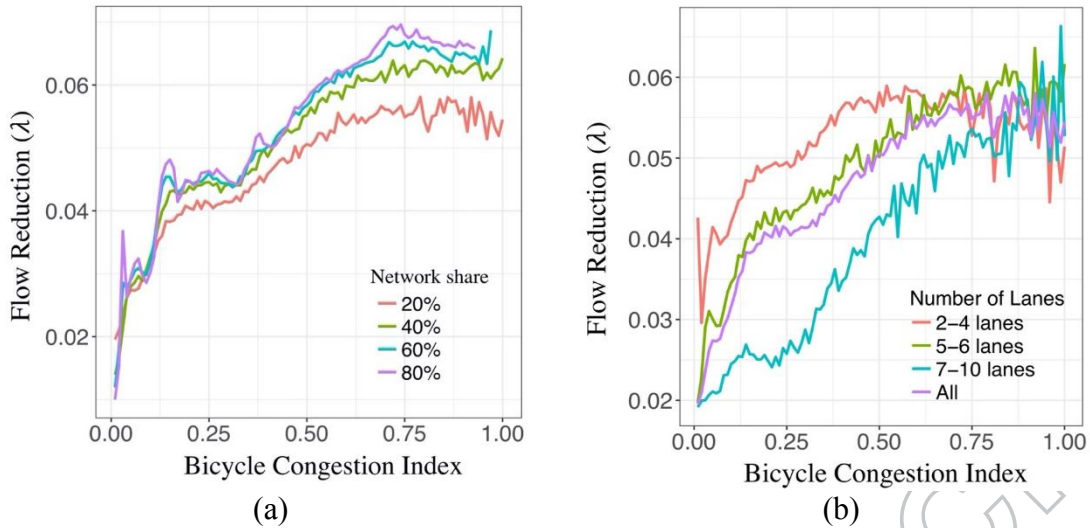


Figure 6. Evolution of λ with respect to BCI and (a) network share; (b) number of lanes.

We now assess the effect of number of car lanes (2-4 lanes; 5-6 lanes; and 7-10 lanes) on the relationship between BCI and λ , which is shown in Figure 6(b). As BCI increases, λ for the 2-4 lanes soars to approximately 0.06 when BCI is around 0.50. Meanwhile, value of λ for networks with larger number of lanes increases much more slowly for the same level of BCI. The results are in line with the assumptions for the link-based method that bicycle traffic mainly affects cars on the right-most lanes and has little impact for wide segments.

Figure 7 compares the relationship for different proportions of car-only roads within sub-network and car flow reductions (λ) under various values of BCI. Note that 25.6% is the average percentage of car-only roads for total sampled sub-networks; 16.4% and 34.4% are the 25th and 75th percentiles, respectively. It is interesting to notice that the difference in λ between networks with few car-only roads and networks with a high percentage of car-only roads is not large (the average difference of λ between the 25th percentile and 75th percentile of car-only roads percentage is 0.0023). Networks with a high percentage of car-only roads have slightly smaller λ only when BCI is between around 0.3 to 0.7. When network bicycle flow is large enough (BCI larger than around 0.7), restricting bicycles cannot increase the network car flow effectively.

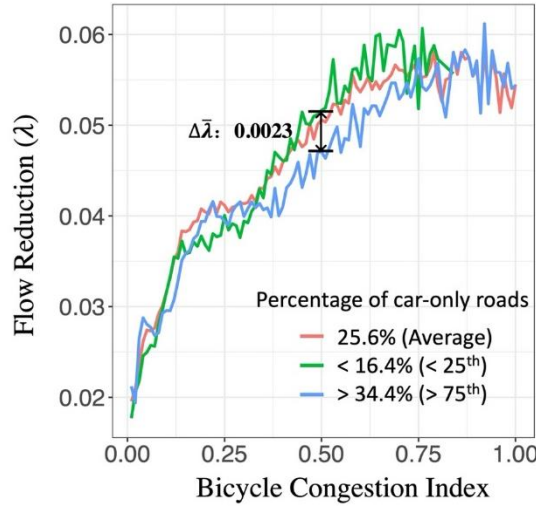


Figure 7. Evolution of λ with respect to BCI and percentage of car-only roads.

Figures 8(a) & 8(b) present the influence of separation type on the relationship between BCI and car flow reduction (λ). Figure 8(a) highlights the impact for different proportion of roads with physical separation (bicycle path); Figure 8(b) demonstrates the influence of different proportion of shared roads. As expected, high percentage of roads with physical separation (more than 66.5%, 75th percentile of total sampled sub-networks) have less flow reduction than networks with fewer physically separated roads. Similarly, higher percentages of shared roads (more than 7.8%, 75th percentile of total sampled sub-networks) have more flow reductions than networks with more separation facilities. Average difference of λ between the 25th and 75th percentiles of physically separated roads is 0.0056 and the value is 0.0058 for shared roads. Compared to increasing car-only roads (the average difference of λ is 0.0023), it is more efficient to decrease the average value of λ by building more physical bicycle facilities, e.g., open space or barriers, and by reducing the percentage of shared roads in the network. As in previous results, when the bicycle flow is large enough, λ value becomes relatively stable and the difference in λ between different shares of separation type is not substantial.

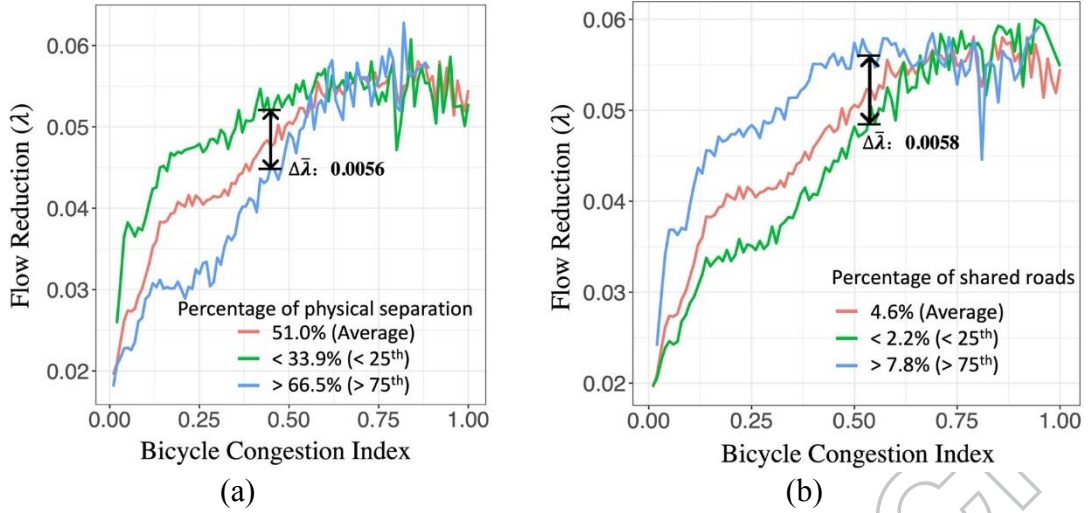


Figure 8. Evolution of λ for BCI and (a) percentage of bicycle path; (b) percentage of shared roads.

4.2 Link-based method

4.2.1 Estimation results

The percentage of spilling behavior (Eq. 9) is estimated using the video data from ten selected segments in Shanghai (five road segments with bicycle path and five road segments with bicycle lane). Each variable is calculated for every 10-minute time slice. Based on the recommended value for capacity of bicycle facility in MOHURD (2012), the maximum capacity $C_{i,max}$ for bicycle path and bicycle lane are set as 1,700 bicycles/h-lane and 1,500 bicycles/h-lane. The average capacity C_i during the 10-minute time slice is modified based on green time/cycle length for segment i : $C_{b,i} = C_{i,max} * Green/Cycle_i$. The estimation results are presented in Table 3. It is shown that car density $k_{c,i}$ has a negative impact on the number of spilling bicycles ($\beta_1 = -0.001$; $p = 0.007$); saturation level of bicycle facilities $q_{b,i}/C_{b,i}$ has positive impact on the number of spilling bicycle ($\beta_2 = 0.346$; $p < 0.001$); bicycle path ($s_i=1$) has significantly lower percentage of spilling bicycles ($\beta_3 = -0.101$; $p = 0.004$) than bicycle lane($s_i=0$).

Table 3. Model estimates for percentage of spilling bicycles (N=238; $R^2=0.617$)

Coefficient	Estimate	S.E.	t value	p value
β_0 (Intercept)	0.090	0.046	1.939	0.057
$\beta_1 (k_{c,i})$	-0.001	0.001	-2.782	0.007
$\beta_2 (q_{b,i}/C_{b,i})$	0.346	0.066	5.243	<0.001
$\beta_3 (s_i)$	-0.101	0.034	-2.965	0.004

Note: s_i is a dummy variable: $s_i=1$ for segments with bicycle path, $s_i=0$ for segments with bicycle lane.

The Greenshields' linear models are empirically estimated based on FCD and LDD for road segments with different road types and number of lanes in Shanghai. To avoid the interference of bicycle, car-only roads and time periods with low network bicycle flow ($BCI < 0.2$) are selected to estimate the results. The estimation results of Greenshields' linear models are shown in Table 3.

Table 3. Estimation results of Greenshields' linear model

Road type	Greenshields' linear model	R^2
Arterial road (L ₂₋₄)	$v_{c,i} = 29.09 (1 - k_{c,i}/102.95)$	0.72
Arterial road (L ₅₋₆)	$v_{c,i} = 23.91 (1 - k_{c,i}/101.91)$	0.51
Arterial road (L ₇₋₁₀)	$v_{c,i} = 26.01 (1 - k_{c,i}/74.88)$	0.43
Secondary road (L ₂₋₄)	$v_{c,i} = 20.45 (1 - k_{c,i}/120.26)$	0.69
Secondary road (L ₅₋₆)	$v_{c,i} = 22.99 (1 - k_{c,i}/91.94)$	0.32

Note: speed limits for arterials and secondary roads are set as 50-60 km/h and 30-40km/h, respectively.

4.2.2 Effect of road facilities

Assuming car traffic are evenly distributed over the network ($q_{b,i} = q_b$), for each network with homogeneous road types and number of lanes, car MFDs without bicycle interference can be estimated based on the estimation results of Greenshields' linear models, as shown in Figure 9. Compared with upper-bound MFDs without eliminating the impact of bicycle traffic, as shown in Figure 3(a), estimated MFDs in Figure 9 have similar shapes but less flow reductions for each network.

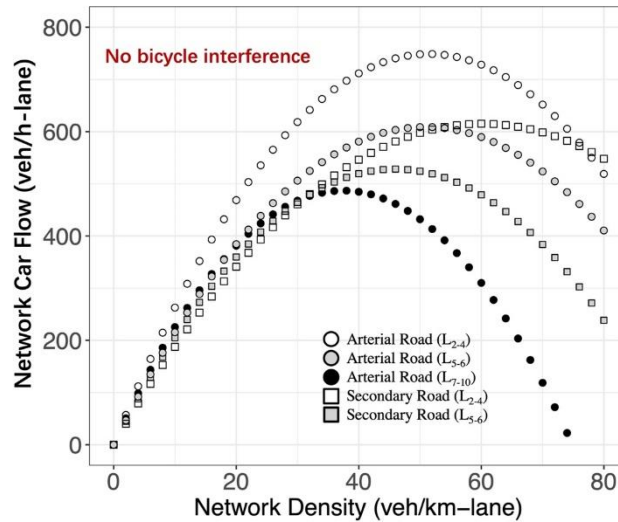
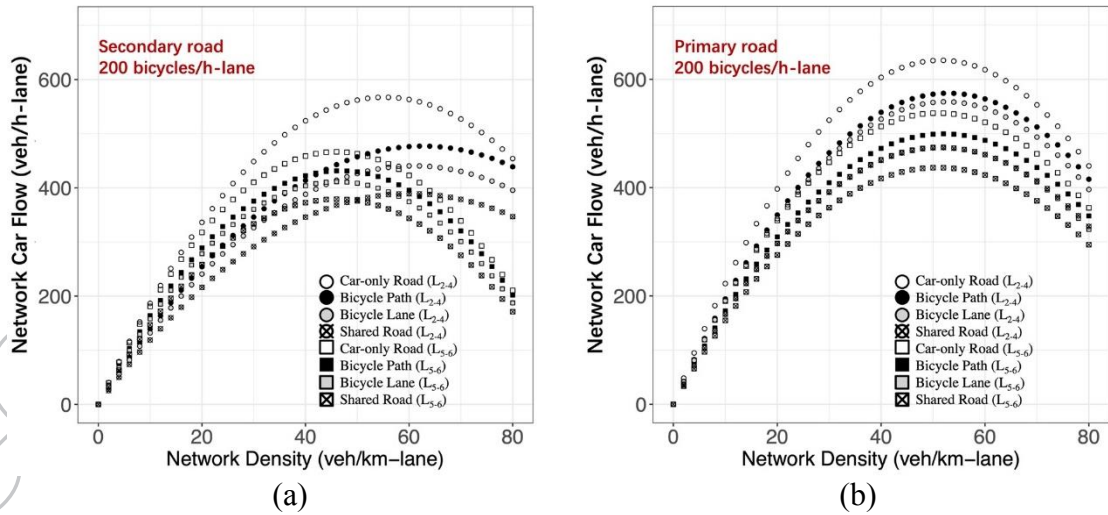


Figure 9. Relationship between road type, number of lanes, and estimated car MFDs.

Based on the spilling-based functional form (Eqs. (8) - (10)), we further estimate car MFDs for networks with homogeneous bicycle facilities (bicycle path, bicycle lane, and

shared lane) and evenly distributed bicycle flow. To calculate the results, more assumptions and estimations are made: average speeds for spilling bicycles $v_{spill,i}$ for each segment are using the free flow speed for bicycles (85th percentile of bicycle travel speed); the value of speed adjustment $\eta(s_{spill,i})$ is extracted from a simulation study that linking number of spilling bicycles and reduction of free flow speed for car traffic (Luo et al., 2015); the threshold between friction interference and block interference is set as 0.01 km, which is consistent with Wierbos et al.(2020); the percentage of violating the bicycle restricted rule δ is estimated by dividing violation records by total cycling records from bicycle-sharing data, and the value is set as a constant (1.8%).

The results of estimated MFDs with different facility types (road type, separation type, and number of lane) and bicycle flow (200 bicycles/h-lane and 400 bicycles/h-lane) are shown in Figures 10(a) - (d). The shapes of MFDs are similar to Figure 3(b) and can well reflect the physical property of car-bicycle interactions: segments with bicycle paths have less flow reductions than segments with bicycle lanes and shared roads; the interference effect of bicycle flow more substantial for narrow segments (2-4 lanes for two directions) than wide segments (5-6 lanes for two directions), especially for conditions of low car density and high bicycle flow; the difference between car-only roads and segments with bicycle path is not substantial for conditions with high car density and low bicycle volume.



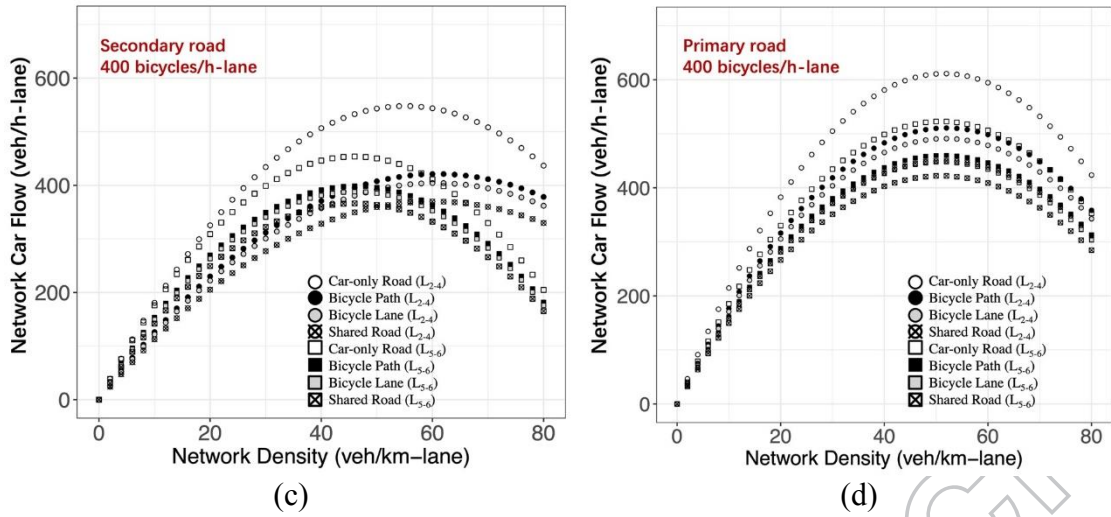


Figure 10. Estimated MFDs for different facility types and bicycle flow: (a) secondary road (200 bicycles/h-lane); (b) secondary road (400 bicycles/h-lane); (c) primary road (200 bicycles/h-lane); (d) primary road (400 bicycles/h-lane).

4.2.3 Relationship between bicycle flow and car flow reduction

Similar to Section 4.1.3, the relationship between bicycle flow and car flow reduction are further investigated using the λ – *trapezoidal* MFD function. Since we have assumed the percentage of violating the bicycle restricted rule δ constant (1.8%) in the previous section, a sensitivity analysis is conducted to reveal how δ impacts the results of flow reduction. Five values of δ (0.1%, 1.0%, 1.8%, 5.0%, and 10.0%) are compared, which are shown in Figure 11(a). The evolutions of λ for various bicycle flow are consistent with Figures 6 to 8. The value of λ increases sharply when the bicycle flow is low and becomes steady when the bicycle flow is large. It is found that decreasing the value of δ can improve the car flow substantially. Since the value of δ is dependent on the local traffic management and route preference of local cyclists, the average value of λ decreases 0.0064 if the percentage of cyclists using car-only roads can be substantially reduced to 0.1% (now 1.8%) by implementing stricter traffic laws and traffic management on these car-only roads. It should be noted that a reduction of δ can also be expected if the ban of cyclists from major roads is lifted and more exclusive bicycle facilities are built in the central area. Cyclists would have safe and fast alternatives to breaking the restricted law.

To reduce car-bicycle interactions and improve network car traffic, several schemes of adjusting existing bicycle facilities are proposed and compared. Since building car-only roads have negative impacts on bicycle traffic (e.g., longer trip length, longer travel

time, more bicycle congestion), we only consider schemes that changing separation types for the existing facilities:

Scheme 1: Keeping the percentage of each separation type unchanged.

Scheme 2: Adding bicycle lanes to the existing shared roads.

Scheme 3: Building physical separation facilities (bicycle path) to the existing shared roads.

Scheme 4: Building physical separation facilities (bicycle path) to the existing bicycle lanes.

Scheme 5: Building physical separation facilities (bicycle path) to the existing bicycle lanes and shared roads.

The performance of different schemes is shown in Figure 11(b). It is indicated that adjusting the separation type (building bicycle lane or bicycle path) for the existing bicycle facilities can decrease car flow reductions substantially, especially for conditions with low bicycle flow (less than about 200 bicycles/h-lane), which is in line with Figure 8(a) and Figures 10(a)-(b). However, as cyclists can spill into car lanes through the gaps of disconnected separation facilities (e.g., the entrance of underground parking/ companies/ shopping malls), the improvement of car traffic is not substantial when the bicycle flow is large. Compared to the results in Figure 11(a), for conditions with high bicycle volume, it is more effective to lift the ban of cyclists from major roads and implement stricter traffic management than only building disconnected bicycle facilities in the central area.

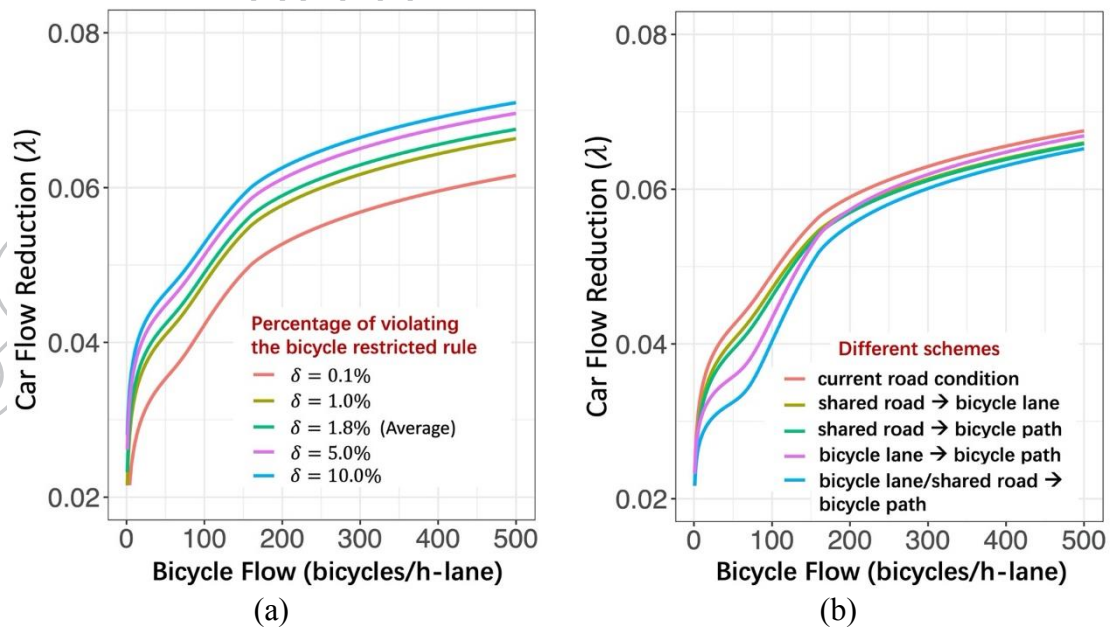


Figure 11. Evolution of λ for bicycle flow with (a) different violation percentage δ ; (b) different schemes of changing separation types.

5 Discussions and Conclusions

This study empirically investigated the car-bicycle interactions at the network level. The impact of bicycle traffic on car MFD was evaluated based on multi-source traffic data, such as taxi FCD data, loop detector data, bicycle GPS data, and video data. The data-driven method and the link-based method were conducted to investigate the impact of bicycle-related facilities and bicycle flow on the shapes of car MFD. It is found that the effect of traffic separation scheme in Shanghai (setting car-only roads) is limited for improving network traffic performance. When comparing the network flow reduction (λ) with London ($\lambda = 0.053$) and Zurich ($\lambda = 0.038$) (Ambühl et al., 2020), Shanghai has more flow reductions, especially for conditions with high bicycle volume. Many factors may affect the results of flow reductions, such as distribution of car demand, signal timing, impact of bus, and impact of non-motorized traffic. The results of this study can be used to improve the network performance by reducing car-bicycle interactions.

Based on the empirical data, we found that the difference of car flow reduction among networks with various percentage of car-only roads is not large. If some road segments are car-only, other road segments within the same network would become more crowded for bicycles, which is prone to increase interactions between bicycle and car flow (Luo et al., 2015). Meanwhile, a small number of cyclists would illegally use car-only roads, which reduces the car flow. Based on the link-based method, the network flow can increase substantially if the percentage of cyclists using car-only roads is reduced to 0.1% (now 1.8%) by implementing stricter traffic laws and management on these car-only roads. The results are consistent with Zacharias (2002), indicating that the total vehicle flow of 55 streets in Shanghai decreased by 24% after the implementation of the car-bicycle separation scheme. Compared with car-only roads, it is more efficient to increase car flow by building more physical bicycle facilities and reducing the percentage of shared roads within the network. If the bicycle facilities are not physically separated, many factors, such as on-street parking occupancy (HCM2010, 2010) and presence of stopped buses (Yang et al., 2009), would increase the spilling behaviors of bicycles and slow down car traffic. However, it should be noted that installing physically separated facilities is less effective for large bicycle volume (more than about 200 bicycles/h-lane). If the bicycle traffic is large enough, cyclists can spill into car lanes through the gaps of disconnected separation facilities (e.g., the entrance of underground

parking/companies/shopping malls) and hinder car traffic. For that case, it is more effective to reduce car-bicycle interactions by lifting the ban of cyclists and implementing stricter traffic management in the central area.

Although the results of this study are promising, both the data-driven and the link-based methods have limitations. As an empirical study on a rather large network (about 80 km²), many important factors, such as facility factors (e.g., roadside parking and bus lanes), signal timing plans, difference of penetration rate among different areas, and impacts from other road users (e.g. bus, e-bikes, and pedestrians) are not controlled or included. For the data-driven method, the bicycle-sharing dataset used is insufficient to fully estimate density or volume of overall bicycle traffic. Due to the limited ranges of empirical car and bicycle data, the data-driven method may not adequately represent the distinct congested branch of the car MFD and conditions of high bicycle flow. The results of the data-driven method can be explained and validated by the link-based method. For the link-based method, the effect of road type, separation type, number of lanes, bicycle flow, and the percentage of cyclists violating the bicycle restricted rule can be controlled. The schemes of implementing stricter traffic management and adjusting separation types may be compared based on the link-based method. However, different from the data-driven method, the link-based method is constructed based on several assumptions, which may simplify the physical property of the two traffic streams. Additionally, since the link-level fundamental diagram are more scattered than MFD (Geroliminis and Daganzo, 2007), the estimation results has relatively low goodness-of-fit and may lead to bias when becoming a network.

Based on the method proposed in this study, we know whether the network performance is at the desired level and understand the potential of improving the network flow by reducing car-bicycle interactions. For the multimodal network in Shanghai, various strategies may be proposed. First, since setting car-only roads has limited improvement for network car flow and would largely reduce bicycle accessibility (e.g., shorter trips, lower travel times), it is recommended to lift the ban of cyclist from these streets. Secondly, building more physically separated facilities between car and bicycle traffic would increase network car flow substantially, especially when the network bicycle flow is not large. Moreover, since the percentage of cyclists violating the bicycle restricted rule in Shanghai is rather high ($\delta = 1.8\%$), the network car flow can also be effectively improved by implementing stricter traffic laws and managements on bicycle traffic. A reduction of δ can also be expected if the ban of cyclists from major roads is

lifted and more exclusive bicycle facilities are built in the central area. The results of this study may also shed light on future 3D-MFD studies for the car-bicycle network. More dynamic multimodal traffic managements can be implemented based on the state of 3D-MFD if the real-time field data of car and bicycle traffic are available.

Acknowledgements

This research was partially supported by the National Nature Science Foundation of China (71971138), the Humanities and Social Science Research Project (No. 19YJAZH077), and Chinese Scholarship Council Scholarship. The authors would like to warmly thank the five anonymous reviewers for their valuable suggestions and comments, which significantly improve the quality of this paper. The authors would also like to express their appreciation to Allister Loder and Kaidi Yang from Institute for Transport Planning and Systems (IVT), ETH Zurich for their valuable suggestions and comments in preparing this manuscript. Any opinions, findings, and conclusions or recommendations expressed in this paper are those of the authors and do not necessarily reflect the views of the sponsors.

References

- Allen, D., J. Hummer, N. Rouphail, and J. Milazzo. 1998. "Effect of bicycles on capacity of signalized intersections." *Transportation Research Record: Journal of the Transportation Research Board* 1646: 87-95.
- Ambühl, L., and M. Menendez. 2016. "Data fusion algorithm for macroscopic fundamental diagram estimation." *Transportation Research Part C:Emerging Technologies* 71: 184-97.
- Ambühl, L., A. Loder, M. Menendez, and K. W. Axhausen. 2017. "Empirical macroscopic fundamental diagrams: Insights from loop detector and floating car data." Paper presented at the 96th Annual Meeting of the Transportation Research Board, Washington, D.C., Jan. 2017.
- Ambühl, L., A. Loder, M. Bliemer, M. Menendez, and K. W. Axhausen. 2018. "Introducing a re-sampling methodology for the estimation of empirical macroscopic fundamental diagrams." *Transportation Research Record: Journal of the Transportation Research Board* 2672 (20): 239-48.

- Ambühl, L., A. Loder, M. Bliemer, M. Menendez, and K. W. Axhausen. 2020. "A functional form with a physical meaning for the macroscopic fundamental diagram." *Transportation Research Part B: Methodological* 137:119-132.
- Ampuntolas, K., N. Zheng, and N. Geroliminis. 2017. "Macroscopic modelling and robust control of bi-modal multi-region urban road networks." *Transportation Research Part B: Methodological* 104: 616-637.
- Ji, Y., H. van Zuylen, and S. Lu. 2016. "Determining the Macroscopic Fundamental Diagram on the Basis of Mixed and Incomplete Traffic Data." Paper presented at the 95th Annual Meeting of the Transportation Research Board, Washington, D.C., Jan. 2016.
- Chen, J., W. Wang, Z. Li, H. Jiang, X. Chen, and S. Zhu. 2014. "Dispersion effect in left-Turning bicycle traffic and its influence on capacity of left-turning vehicles at signalized intersections." *Transportation Research Record: Journal of the Transportation Research Board* 2468: 38-46.
- Chen, Q., and Y. Wang. 2016. "A cellular automata (CA) model for motorized vehicle flows influenced by bicycles along the roadside." *Journal of Advanced Transportation* 50: 949-966.
- Chen, J., Z. Li, H. Jiang, S. Zhu, and W. Wang. 2017. "Simulating the impacts of on-street vehicle parking on traffic operations on urban streets using cellular automation." *Physica A: Statistical Mechanics and Its Applications* 468: 880-891.
- Chen, J., Z. Li, W. Wang, and H. Jiang. 2018. "Evaluating bicycle-vehicle conflicts and delays on urban streets with bike lane and on-street parking." *Transportation Letters* 10 (1): 1-11.
- Daganzo, C. F. 2007. "Urban gridlock: Macroscopic modeling and mitigation approaches." *Transportation Research Part B: Methodological* 41(1): 49-62.
- Daganzo, C. F., and N. Geroliminis. 2008. "An analytical approximation for the macroscopic fundamental diagram of urban traffic." *Transportation Research Part B: Methodological* 42(9): 771-781.
- Ding, H., F. Guo, X. Zheng, and W. Zhang. 2017. "Traffic guidance-perimeter control coupled method for the congestion in a macro network." *Transportation Research Part C: Emerging Technologies* 81: 300-316.
- Duan, J. L., R. J. Li, L. Hou, W. J. Wang, G. F. Li, S. E. Li, B. Cheng, and H. B. Gao. 2017. "Driver braking behavior analysis to improve autonomous emergency braking

- systems in typical Chinese vehicle-bicycle conflicts." *Accident Analysis & Prevention* 108: 74-82.
- Edie, L.C. 1963. "Discussion of Traffic Stream Measurements and Definitions. " Paper presented at the 2nd International Symposium on the Theory of Traffic Flow, London, June 1963.
- Fu, H., X. Tang, Y. Wang, N. Zheng, and N. Geroliminis. 2018. "Empirical Analysis of Large-Scale Multimodal Traffic with Multisensor Data: A Case Study in the Shenzhen Network." Paper presented at the 97th Annual Meeting of the Transportation Research Board, Washington, D.C., Jan. 2018.
- Gang, R., H. Jiang, J. Chen, Z. Huang, and L. Lu. 2016. "Heterogeneous cellular automata model for straight-through bicycle traffic at signalized intersection." *Physica A: Statistical Mechanics and its Applications* 451: 70-83.
- Gayah, V. V., and C. F. Daganzo. 2011. "Clockwise hysteresis loops in the Macroscopic Fundamental Diagram: An effect of network instability." *Transportation Research Part B: Methodological* 45 (4): 643-55.
- Geroliminis, N., and C. F. Daganzo. 2007. "Macroscopic modeling of traffic in cities." Paper presented at the 86th Annual Meeting of the Transportation Research Board, Washington, D.C., Jan. 2007.
- Geroliminis, N., and C. F. Daganzo. 2008. "Existence of urban-scale macroscopic fundamental diagrams: Some experimental findings." *Transportation Research Part B: Methodological* 42(9): 759-70.
- Geroliminis, N., and J. Sun. 2011. "Properties of a well-defined macroscopic fundamental diagram for urban traffic." *Transportation Research Part B: Methodological* 45 (3): 605-617.
- Geroliminis, N., N. Zheng, and K. Ampountolas. 2014. "A three-dimensional macroscopic fundamental diagram for mixed bi-modal urban networks." *Transportation Research Part C: Emerging Technologies* 42: 168-81.
- Highway Capacity Manual 2010 (HCM 2010). Transportation Research Board of the National Academies. 2010. Washington, DC: The Board.
- Hoogendoorn, S. P., M. C. Campanella, and W. Daamen. 2010. "Macroscopic fundamental diagrams for pedestrian networks. " Paper presented at the 89th Annual Meeting of the Transportation Research Board, Washington, D.C., Jan. 2010.
- Huang, Y., D. Sun, N. Garrick, and K.W. Axhausen. 2018a. "Evaluating Shanghai's non-local vehicle restriction policy using the empirical macroscopic fundamental

- diagram." Paper presented at the 18th Swiss Transport Research Conference, Ascona, May 2018.
- Huang, Y., D. Sun, and L. Zhang. 2018b. "Effects of congestion on drivers' speed choice: Assessing the mediating role of state aggressiveness based on taxi floating car data." *Accident Analysis & Prevention* 117: 318-327.
- Huang Y., D. Sun, and J. Tang. 2018c. "Taxi driver speeding: who, when, where and how? A comparative study between Shanghai and New York City." *Traffic Injury Prevention* 19(3): 311-316.
- Ji, Y., J. Luo, and N. Geroliminis. 2014. "Empirical Observations of Congestion Propagation and Dynamic Partitioning with Probe Data for Large-Scale Systems." *Transportation Research Record: Journal of the Transportation Research Board* 2422(1): 1-11.
- Kim, S., and H. Yeo. 2017. "Evaluating link criticality of road network based on the concept of macroscopic fundamental diagram." *Transportmetrica A: Transport Science* 13(2): 162-193.
- Knoop, V. L., H. V. Lint, and S.P. Hoogendoorn. 2015. "Traffic dynamics: Its impact on the macroscopic fundamental diagram." *Physica A: Statistical Mechanics and Its Applications* 438: 236-250.
- Koenker, R., and J. Machado. 1999. "Goodness of fit and related inference processes for quantile regression." *Journal of the American Statistical Association* 94 (448): 1296-1310.
- Lawrence, B. M., J. A. Oxley, D. B. Logan, and M. R. Stevenson. 2018. "Cyclist exposure to the risk of car door collisions in mixed function activity centers: A study in Melbourne, Australia." *Traffic Injury Prevention* 19: S164-S8.
- Loder, A., L. Ambühl, M. Menendez, and K. W. Axhausen. 2017. "Empirics of multi-modal traffic networks - Using the 3D macroscopic fundamental diagram." *Transportation Research Part C: Emerging Technologies* 82: 88-101.
- Loder, A., L. Ambühl, M. Menendez, and K. W. Axhausen. 2019. "Understanding traffic capacity of urban networks." *Scientific Reports* 9(1): 1-10.
- Luo, Y., B. Jia, J. Liu, W.H.K. Lam, X. Li, and Z. Gao. 2015. "Modeling the interactions between car and bicycle in heterogeneous traffic." *Journal of Advanced Transportation* 49(1): 29-47.

- Ministry of Housing and Urban-Rural Development of China (MOHURD). 2012. *Code for design of urban road engineering(CJJ37-2012)*. Beijing: China Architecture & Building Press.
- Nian, G.Y., F. Chen, Z. Li, Y. Zhu, and D.J. Sun. 2019. "Evaluating the alignment of new metro line considering network vulnerability with passenger ridership." *Transportmetrica A: Transport Science* 15(2): 1402-1418.
- Park, E., S. Turner, and C. Spiegelman. 2003. "Empirical approaches to outlier detection in intelligent transportation systems data." *Transportation Research Record: Journal of the Transportation Research Board* 1840:87-95.
- Piatkowski, D. P., W. Marshall, and A. Johnson. 2017. "Identifying behavioral norms among bicyclists in mixed-traffic conditions." *Transportation Research Part F: Traffic Psychology and Behaviour* 46:137-48.
- Schepers, J.P., P.A. Kroeze, W. Sweers, and J.C. Wüst. 2011. "Road factors and bicycle-motor vehicle crashes at unsignalized priority intersections." *Accident Analysis & Prevention* 43(3): 853-61.
- Shanghai Urban Rural Construction and Transportation Development Research Institute (SURCTD). 2015. *The 5th Shanghai Comprehensive Transport Survey*. Shanghai.
- Silvano, A. P., H. N. Koutsopoulos, and X. L. Ma. 2016. "Analysis of vehicle-bicycle interactions at unsignalized crossings: A probabilistic approach and application." *Accident Analysis & Prevention* 97: 38-48.
- Sun, D.J., L. Elefteriadou. 2010. "Research and implementation of lane-changing model based on driver behavior." *Transportation Research Record: Journal of the Transportation Research Board* 2161: 1-10.
- Sun, D.J., L. Elefteriadou. 2014. "A driver behavior based lane-changing model for urban arterial streets." *Transportation Science* 48(2): 184-205.
- Sun, D.J., K. Zhang, and S. Shen. 2018. "Analyzing spatiotemporal traffic line source emissions based on massive didi online car-hailing service data." *Transportation Research Part D: Transport and Environment* 62: 699-714.
- Sun D.J., and X. Ding. 2019. "Spatiotemporal evolution of ridesourcing markets under the new restriction policy: A case study in Shanghai." *Transportation Research Part A: Practice and Police* 130: 227-239.
- Taherifar, N., H. Hamedmoghadam, S. Sree, and M. Saberi. 2019. "A macroscopic approach for calibration and validation of a modified social force model for

- bidirectional pedestrian streams." *Transportmetrica A: Transport Science* 15(2): 1637-1661.
- Vasic, J., and H. Ruskin. 2012. "Cellular automata simulation of traffic including cars and bicycles." *Physica A: Statistical Mechanics and Its Applications* 391(8): 2720-9.
- Wang, X., H. Liu, R. Yu, B. Deng, X. Chen, and B. Wu. 2014. "Exploring operating speeds on urban arterials using floating car data: Case study in Shanghai." *Journal of Transportation Engineering* 140(9): 04014044.
- Wei, B., and D.J. Sun. 2018. "A two-layer network dynamic congestion pricing based on Macroscopic Fundamental Diagram." *Journal of Advanced Transportation* 2018(2): 1-11.
- Wierbos, M. J., V. L. Knoop, F. S. Hänseler, and S. P. Hoogendoorn. 2020. "A macroscopic flow model for mixed bicycle-car traffic." *Transportmetrica A: Transport Science* DOI: 10.1080/23249935.2019.1708512
- Xie, D. F., D. Z. Wang, and Z. Y. Gao. 2016. "Macroscopic analysis of the fundamental diagram with inhomogeneous network and instable traffic." *Transportmetrica A: Transport Science* 12(1): 20-42.
- Xin, C. J. 1996. "Bicycle transportation in Shanghai: status and prospects." *Transportation Research Record: Journal of the Transportation Research Board* 1563: 8-15.
- Yang, X., Z. Gao, X. Zhao, and B. Si. 2009. "Road capacity at bus stops with mixed traffic flow in China." *Transportation Research Record: Journal of the Transportation Research Board*. 2111: 18-23.
- Yuan, K., Victor L. K., and S. P. Hoogendoorn. 2019. "Multi-class traffic flow on a partially space-shared road." *Transportmetrica B: Transport Dynamics* 7(1): 1505-1520.
- Zacharias, J. 2002. "Bicycle in Shanghai: movement patterns, cyclist attitudes and the impact of traffic separation." *Transport Reviews* 22 (3): 309-22.
- Zhang, Y., and Z. Mi. 2018. "Environmental benefits of bike sharing: A big data-based analysis." *Applied Energy* 220: 296-301.
- Zheng, N., and N. Geroliminis. 2013. "On the distribution of urban road space for multimodal congested networks." *Transportation Research Part B: Methodological* 57(C): 326-41.

Zheng, N., and N. Geroliminis. 2016. "Modeling and optimization of multimodal urban networks with limited parking and dynamic pricing." *Transportation Research Part B: Methodological* 83: 36-58.

ACCEPTED MANUSCRIPT

APPENDIX 1 MODIFICATION OF TAXI PENETRATION RATE

Spatial bias may exist when applying estimated penetration rate from the highway network $\hat{\rho}_H$ directly to surface roads $\hat{\rho}_S$. According to the 5th Shanghai Comprehensive Transport Survey (SURCTD, 2015), the average travel distance for each taxi trip is about 7.1 km, while for a regular car, it is about 14.5 km. Different travel distance may lead to other route preferences, which may result in varying taxi penetration rates between highways and surface road networks. Consequently, route choice (elevated highway or surface road) for drivers with different travel distance distribution is expected to modify taxi penetration rate for surface roads. As regular drivers' trajectories are not available in this study, some operational taxi trips were selected to represent regular drivers' trips, defined as quasi-normal trips. The travel distance for these quasi-normal trips is assumed to obey the same type of travel distance distribution with taxi trips and the average travel distance for these quasi-normal trips is as same as regular drivers (14.5 km). The process of modifying the taxi penetration rate for surface road $\hat{\rho}_S$ is illustrated as follows:

First, we need to select a suitable distance distribution for taxi trips and quasi-normal trips. The distance distribution for taxi trips is compared to the Weibull distribution, Lognormal distribution and Gamma distribution, respectively, with estimation results shown in Figure A1. From the Q-Q and P-P plots, Gamma distribution best captures distance distribution for taxi drivers. Moreover, AIC and BIC values of Gamma distribution are lower than those for the Weibull and lognormal distributions.

Goodness-of-fit criteria	Weibull distribution	Lognormal distribution	Gamma distribution
AIC	633708.8	628886.0	628460.4
BIC	633728.1	628905.3	628479.7

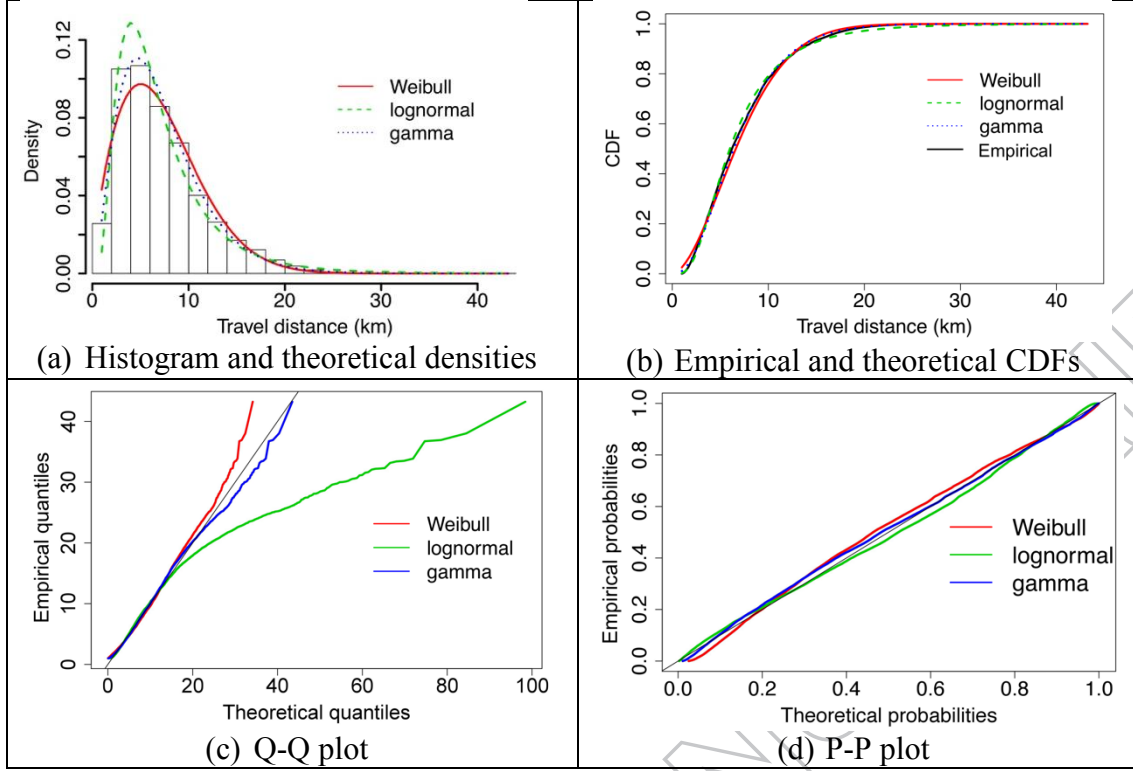


Figure A1 Fitting results of travel distance distribution ($n=114,452$ trips)

Supposing that each trip distance x follows a Gamma distribution with shape parameter k and rate parameter θ , the probability density function of travel distance $f(x)$ can be described as:

$$f(x) = \frac{\theta^k}{\Gamma(k)} x^{k-1} e^{-x\theta}, \quad x > 0 \quad (11)$$

where $\Gamma(k)$ is the Gamma function, defined as $\Gamma(k) = \int_0^\infty s^{k-1} e^{-s} ds$, $k > 0$. Mean travel distance distribution can be then calculated as $\mathbb{E}(x) = k/\theta$.

For taxi drivers, the fitting results show that their travel distance distribution obeys the Gamma distribution with shape parameter $k^T = 2.8329$ ($S.E. = 0.0162$) and rate parameter $\theta^T = 0.3775$ ($S.E. = 0.0024$). For regular drivers, we assume that travel distance distribution of regular drivers also obeys the Gamma distribution and has the same shape parameter as taxi drivers' ($k^R = k^T = 2.8329$). Since the average single

travel distance for regular drivers $\mathbb{E}(x)^R$ is 14.5 km (SURCTD, 2015), the rate parameter for regular drivers θ^R can be estimated as $\theta^R = \theta^T \cdot \mathbb{E}(x)^T / \mathbb{E}(x)^R = 0.1953$.

To represent quasi-normal trips, we calculate the travel distance for each operational taxi trip and select operational taxi trips that obey Gamma distribution with shape parameter $k^R = 2.8329$ and rate parameter $\theta^R = 0.1953$. For example, if we want to draw N taxi trips to represent quasi-normal trips, we can determine the number of quasi-normal trips for each distance group as $N \cdot f_R(x)$, where $f_R(x)$ is the percentage of each distance group x according to the estimated Gamma distribution for regular drivers. Then, operational taxi trips with corresponding distance x are randomly selected to form each distance group. Note that unoccupied taxi trips are not included since these taxis prefer to use surface roads and would make a detour to hunt passengers, which cannot represent regular drivers well. Random seeds from 1 to 100 (one random seed for each distribution) are used to select 100 groups of taxi drivers and regular drivers that follow the corresponding distance distributions. Each group consists of 10,000 taxi trips and 10,000 quasi-normal trips. Relationships between travel distance and proportion of length using elevated highways for both taxi trips $P_T(x)$ and quasi-normal trips $P_R(x)$ are estimated for each group. Finally, the total taxi travel distance on highways is estimated as $d_{T,H}^{tot} = \sum_x D_T f_T(x) P_T(x)$, where D_T is the daily taxi travel distance for all taxis from Qiangsheng Company (3,234,000 km), $f_T(x)$ is the percentage of each travel distance x . The total taxi travel distance on surface roads is estimated as $d_{T,S}^{tot} = \sum_x D_T f_T(x) (1 - P_T(x))$. Similarly, for regular drivers, the total highway travel distance is estimated as $d_{R,H}^{tot} = \sum_x D_R f_R(x) P_R(x)$, where D_R is the daily travel distance for all regular drivers (97,150,000 km) (SURCTD, 2015), $f_R(x)$ is the percentage of each travel distance; the travel distance on surface roads is estimated as $d_{R,S}^{tot} = \sum_x D_R f_R(x) (1 - P_R(x))$.

According to Edie's generalized traffic definition, the taxi penetration rate on highway $\hat{\rho}_H$ can be estimated as $\hat{\rho}_H = \hat{q}_{T,H}/\hat{q}_H = d_{T,H}^{tot}/(d_{T,H}^{tot} + d_{R,H}^{tot})$, where $\hat{q}_{T,H}$ is the taxi flow for highway; \hat{q}_H is the total traffic flow for highway. The taxi penetration rate on surface road can be estimated as $\hat{\rho}_S = \hat{q}_{T,S}/\hat{q}_S = d_{T,S}^{tot}/(d_{T,S}^{tot} + d_{R,S}^{tot})$, where $\hat{q}_{T,S}$ is the taxi flow for surface road; \hat{q}_S is the total traffic flow for surface road. The modification factor can thus be estimated by $\gamma = \hat{\rho}_H/\hat{\rho}_S$ from 100 groups of data. Estimation result for γ is 0.5653 ($S.E. = 0.0009$, $R^2=0.9997$).

Based on the highway penetration rate $\hat{\rho}_H$ estimated by Eq. (5), the average taxi penetration rate for surface roads $\bar{\rho}_S$ is 3.65%. Based on field surveys from 40 selected arterial/secondary roads in Shanghai, Sun et al. (2018) demonstrated that the average taxi penetration rate on surface roads is approximately 12.9%, with no large differences across the zones and road types. However, the results of Sun et al. (2018) is based on all taxi companies in Shanghai (about 49,788 vehicles) while the results of this study is merely based on taxis from Shanghai Qiang-Sheng Taxi Company, with about 13,475 vehicles. After modification for the overall number of taxis, the average surface road penetration rate ($3.65\% \times 49,788 / 13,475 = 13.5\%$) is very close to that in Sun et al. (2018) (12.9%).

APPENDIX 2 SUPPLEMENTAL FIGURES

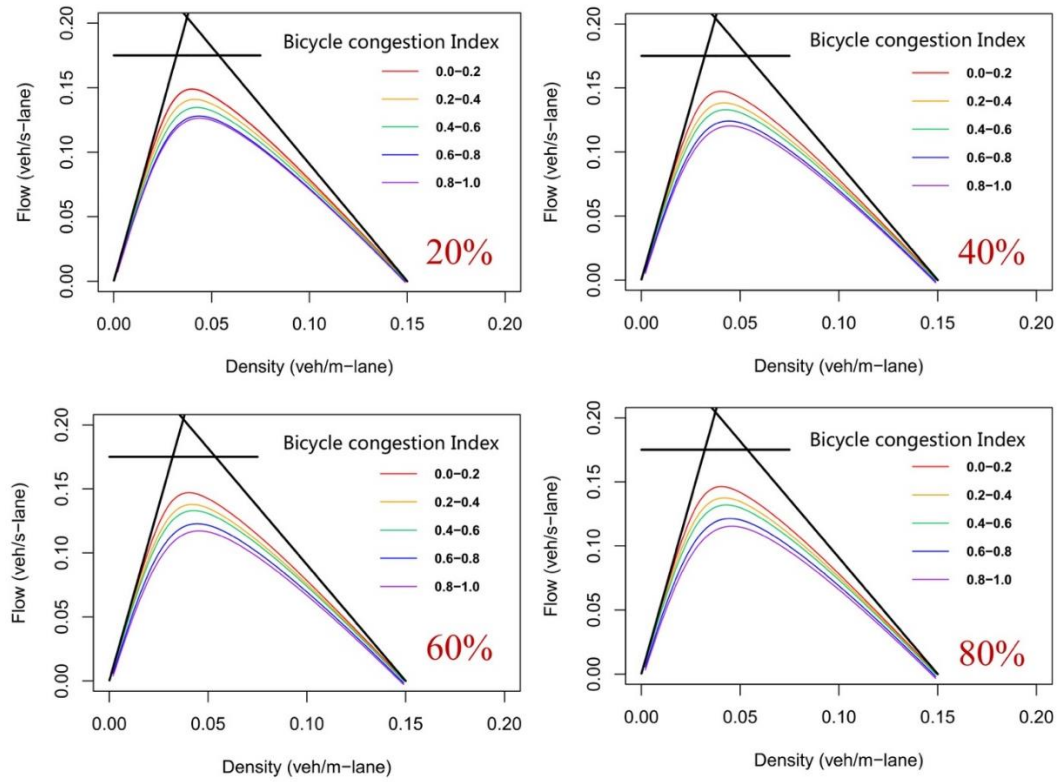


Figure A2 λ – *trapezoidal* MFDs for different network shares.